



## Did Holocene climate changes drive West Antarctic grounding line retreat and re-advance?

5 Sarah U. Neuhaus<sup>1</sup>, Slawek M. Tulaczyk<sup>1</sup>, Nathan D. Stansell<sup>2</sup>, Jason J. Coenen<sup>2</sup>, Reed P. Scherer<sup>2</sup>, Jill A. Mikucki<sup>3</sup>, Ross D. Powell<sup>2</sup>

<sup>1</sup>Earth and Planetary Sciences, University of California Santa Cruz, Santa Cruz, CA, 95064, USA

<sup>2</sup>Department of Geology and Environmental Geosciences, Northern Illinois University, DeKalb, IL, 60115, USA

<sup>3</sup>Department of Microbiology, University of Tennessee Knoxville, Knoxville, TN, 37996, USA

10

*Correspondence to:* Sarah U. Neuhaus (suneuhau@ucsc.edu)

**Abstract.** Knowledge of past ice sheet configurations is useful for informing projections of future ice sheet dynamics and for calibrating ice sheet models. The topology of grounding line retreat in the Ross Sea Sector of Antarctica has been much debated, but it has generally been assumed that the modern ice sheet is as small as it has been for more than 100,000 years (Conway et al., 1999; Lee et al., 2017; Lowry et al., 2019; McKay et al., 2016; Scherer et al., 1998). Recent findings suggest that the West Antarctic Ice Sheet (WAIS) grounding line retreated beyond its current location earlier in the Holocene and subsequently re-advanced to reach its modern position (Bradley et al., 2015; Kingslake et al., 2018). Here, we further constrain the post-LGM grounding line retreat and re-advance in the Ross Sea Sector using a two-phase model of radiocarbon input and decay in subglacial sediments from six sub-ice sampling locations. In addition, we reinterpret high basal temperature gradients, measured previously at three sites in this region (Engelhardt, 2004), which we explain as resulting from recent ice shelf re-grounding accompanying grounding line re-advance. At one location – Subglacial Lake Whillans (SLW) – for which a sediment porewater chemistry profile is known, we estimate the grounding line re-advance by simulating ionic diffusion. Collectively, our analyses indicate that the grounding line retreated over SLW ca. 4000 years ago, and over sites on Whillans Ice Stream (WIS), Kamb Ice Stream (KIS), and Bindschadler Ice Stream (BIS) ca. 4500, ca. 2000, and ca. 2000 years ago respectively. The grounding line only recently re-advanced back over those sites ca. 1000, ca. 1100, ca. 500, and ca. 500 years ago for SLW, WIS, KIS, and BIS respectively. The timing of grounding line retreat coincided with a warm period in the mid- to late-Holocene. Conversely, grounding line re-advance is coincident with climate cooling in the last 1000-2000 years. Our estimates for the timing of grounding line retreat and re-advance are also consistent with relatively low carbon-to-nitrogen ratios measured in our subglacial sediment samples (suggesting a marine source of organic matter) and with the lack of grounding-zone wedges in front of modern grounding lines. Based on these results, we propose that the Siple Coast grounding line motions in the mid- to late-Holocene were driven by relatively

25  
30



modest changes in regional climate, rather than by ice sheet dynamics and glacioisostatic rebound, as hypothesized previously (Kingslake et al., 2018).

## 35 1 Introduction

Ice loss from the West Antarctic Ice Sheet (WAIS) is a significant uncertainty in projections of near-future sea-level rise (Bamber et al., 2019; Church et al., 2013). This uncertainty is partly due to limited observational constraints on the climate sensitivity of WAIS grounding lines, which mark the locations where ice thins and starts floating on seawater. The evolution of grounding line positions in West Antarctica during and immediately following the Last Glacial Maximum (LGM) is well documented because the relevant geologic evidence is largely accessible to marine geophysical and geological investigations (Anderson et al., 2014). However, evidence of WAIS grounding lines during much of the Holocene is hidden underneath fringing ice shelves, or even beneath the ice sheet itself (e.g., Bradley et al., 2015; Kingslake et al., 2018). For a long time, the scientific consensus has been that the modern configuration of WAIS is its smallest since the LGM (Anderson et al., 2014; Bentley et al., 2014; Conway et al., 1999; Hall et al., 2013). However, recent findings suggest that during the Holocene, at least some of WAIS grounding lines retreated behind their modern positions before re-advancing to their current location (Bradley et al., 2015; Kingslake et al., 2018).

Understanding Holocene ice sheet behavior may aid current efforts to project near-future ice mass loss from WAIS, due to the similarity of Holocene climatic and glacioisostatic forcings to the modern and near-future conditions. Here we re-examine previously collected datasets and samples to estimate the timing of grounding line retreat from, and re-advance to, the modern configuration in the Ross Sea sector of WAIS. We show that the available evidence is consistent with a climatic forcing of these major grounding line movements, with the retreat occurring during warm periods of the Holocene (Cuffey et al., 2016), which are also characterized by a decrease in sea-ice cover in the Ross Sea (Hall et al., 2006). Re-advance occurred in the last 2000 years, corresponding to cooling recorded in the WAIS Divide ice core and an increase in Ross Sea summertime sea ice (Cuffey et al., 2016; Hall et al., 2006). Ice sheet model results published in Kingslake et al. (2018) suggest that these changes in Holocene positions of WAIS grounding lines may have been associated with global sea-level variations of about 0.2-0.3 m at the time when temperature variations at the WAIS Divide ice core site amounted to just a few degrees (Cuffey et al., 2016; Cuffey, 2017). Previous research in Greenland has indicated that at least some of the Greenland Ice Sheet retreated behind its present margin during the mid-Holocene climatic optimum (Vasskog et al., 2015). Greenland Ice Sheet simulations suggest that this contributed an equivalent of 0.1-0.3 m of global sea-level rise (ibid.).

60



## 2 Methods

### 2.1 Modelling of Basal Temperature Gradients

The work of Engelhardt (2004) highlighted the fact that a large fraction of vertical temperature profiles measured along the Siple Coast are difficult to explain with an assumption of climatic and ice dynamic steady state because observed basal temperature gradients are anomalously high. Here, we conjecture that this unsteady thermal state is due to Holocene ice shelf re-grounding in the region (Kingslake et al., 2018). Thus, we modelled the evolution of basal temperature gradients to constrain the timing of ice shelf grounding consistent with observed high basal temperature gradients. Measurements and analysis of temperature profiles taken at our field sites have previously been published (Engelhardt, 2004; Engelhardt and Kamb, 1993; Kamb, 2001), but we re-analyzed them with the new assumption that this area was an ice shelf that grounded in the recent past. We focused on the sites that had very steep basal temperature gradients: Kamb Ice Stream (KIS), Bindschadler Ice Stream (BIS), and the Unicorn (UC) (Fig. 1). (N.B. In this paper we will distinguish between our field sites and the ice streams they are located on by using abbreviations to refer to the field sites, and full names to refer to the ice streams.) Building on modelling employed by Bindschadler et al. (1990) to date the formation of Crary Ice Rise as the Ross Ice Shelf grounded on a bathymetric high, we modelled temperature profiles of an ice shelf before and after grounding. We then compared the resulting basal temperature gradients to observed basal temperature gradients (Engelhardt, 2004). Our MATLAB code solves a one-dimensional, forward Euler, vertical advection-diffusion equation with a one-year time step and 10 m vertical step chosen to satisfy the von Neumann stability condition. The accumulation rate is set to be equal to the sum of vertical advection and change in ice thickness. Thus, when ice thickness remains constant, vertical advection is equal to the accumulation.

We ran the ice temperature model in two phases: floating ice shelf and grounded ice. First, we ran a diffusion advection model for the ice shelf phase with a constant surface temperature of  $-25\text{ }^{\circ}\text{C}$  based on surface temperature measurements along the Siple Coast (Engelhardt, 2004) and a bottom temperature equal to the freezing point of seawater at a salinity of 34 PSU and a pressure corresponding to ice thickness, calculated using Eq. (5) in Begeman et al. (2018). We assumed a constant surface accumulation rate of 0.15 m/yr based on observations at Siple Dome (Waddington et al., 2005). Additionally, we assumed the ice shelf to be in steady state, which requires a basal melt rate of 0.15 m/yr to compensate for accumulation and ignored horizontal advection. We varied the starting ice shelf thickness from 500 m to 1000 m and allowed the ice shelf temperature profile to come to steady state. Using this ice shelf steady-state temperature profile as the initial conditions for phase two of the simulations, we then modelled the ice temperature evolution after grounding. Keeping the surface boundary conditions constant, we changed the bottom temperature boundary condition to reflect the pressure melting point of ice. Although other similar models – including the Bindschadler et al. (1990) model – pick the basal boundary condition after grounding to be the geothermal flux, we chose the freezing point of water because we assumed that basal freeze-on occurred at these locations after grounding, as evidenced by the widespread presence of basal ice layers found in boreholes drilled along the Siple Coast ice streams



(Christoffersen et al., 2010; Kamb, 2001; Vogel et al., 2005) and at the grounding zone of the Whillans Ice Stream  
95 (unpublished data). In addition, we calculated the thickness of basal ice that forms during Phase 2 of the model. We  
allowed the model to run from 0 to 10,000 years, and obtained the time-dependent temperature gradient for the bottom 100  
m so we could compare our modelled results to observed basal temperature gradients (cf. Engelhardt, 2004). We chose  
10,000 years ago as the earliest the grounding line could have advanced over our field sites based on the grounding line  
retreat/re-advance models presented in Kingslake et al. (2018). Sensitivity tests and equations used for our ice temperature  
100 model are presented in the Supplemental Material.

## 2.2 Ionic Diffusion Modelling

To estimate the timing of retreat and re-advance of the grounding line at Subglacial Lake Whillans (SLW) (Fig. 1),  
where the observed basal temperature gradients are not anomalously steep (Fisher et al., 2015), we compared measured  
porewater ionic concentrations from a sediment core collected at SLW (Michaud et al., 2016a) to values modelled using an  
105 ionic diffusion model with a two-stage upper boundary condition. The first phase here assumes that the sedimentary column  
at SLW was exposed to seawater for some length of time during the Holocene ( $T_o$ ). This was followed by ice-shelf re-  
grounding and exposure of the SLW sedimentary column to basal meltwater ( $T_i$ ). Porewater chemistry data that we compare  
to the output of our forward model comes from sediment core MC-3B collected from SLW using a multicorer on January 30,  
2013; methods used for sediment core and porewater collection are described in detail in Tulaczyk et al. (2014) and Michaud  
110 et al. (2016b).

We ran one-dimensional vertical diffusion simulations using the chemical parameters  $\text{Cl}^-$ ,  $\text{SO}_4^{2-}$ ,  $\text{Na}^+$ ,  $\text{Ca}^{2+}$ ,  $\delta^{18}\text{O}$ ,  
and  $\partial\text{D}$ , through pore spaces of sediments below SLW (e.g. Adkins and Schrag, 2003). The diffusion coefficients used for  
each chemical parameter examined in this study were calculated using the equation from Li and Gregory (1974) for diffusion  
of ions through sediments:

115

$$D_{sed} = D \frac{\alpha}{\theta^2} \quad (1)$$

Where  $D$  is the self-diffusion coefficient,  $\alpha$  is the ratio of viscosity of the bulk solution to the average viscosity of the  
interstitial solution and  $\theta$  is tortuosity.  $\alpha$  is a constant with value close to one (Li and Gregory, 1974). In this study we  
120 assume it to be exactly one for simplicity. We used previously calculated self-diffusion coefficients determined for the  
chemical parameters at 0 °C (Li and Gregory, 1974; Wang, 1951a, 1951b). To calculate tortuosity, we use an equation from  
Boudreau (1996):

$$\theta^2 = 1 - \ln(\varphi^2) \quad (2)$$

125



Where  $\varphi$  represents porosity, which is taken to be 0.4 here (Engelhardt et al., 1990; Tulaczyk et al., 2001). The final diffusion coefficients used for each chemical parameter are shown in Table (1).

We forced the diffusion model by switching the upper boundary conditions to reflect either marine or subglacial conditions (Table 1), which represent time periods when the grounding line had retreated beyond or advanced over SLW, respectively. The depth of the simulated diffusion profile was 100 m, vertical resolution was 0.5 m, and temporal resolution was 1 year. We started each simulation assuming that the initial porewater through the entire profile was in equilibrium with subglacial meltwater conditions, i.e. meltwater chemical properties of Subglacial Lake Whillans (Table 1) throughout the domain thickness. This assumption is justified by the fact that the SLW site was beneath the ice sheet for at least 30,000 years (Clark et al., 2009) and must have been in a subglacial setting for almost all of the Quaternary period when WAIS was mostly larger than today (e.g., Scherer et al., 1998). We then instantaneously changed the upper boundary condition at time  $t = 0$  to reflect seawater values (Table 1) to represent post-LGM grounding line retreat past SLW. In this first phase, characterized by simple initial and boundary conditions, the time- and depth-dependent changes in chemical concentration for each parameter can be expressed using the analytical solution (Turcotte and Schubert, 2014, Eq. 4.113):

140

$$\frac{C-C_o}{C_s-C_o} = \operatorname{erfc}\left(\frac{y}{2\sqrt{D_{sed}t}}\right) \quad (3)$$

Where  $C$  is the ion or isotope concentration, subscripts  $o$  and  $s$  represent initial and surface respectively,  $y$  is the distance from the surface, and  $t$  is the total time. We then instantaneously changed the boundary conditions at time  $t = T_o$  back to subglacial meltwater conditions to simulate ice shelf re-grounding. At  $t = T_o$  we also switch to solving the problem using a finite-difference diffusion model, which is a modified version of the same MATLAB code used by us previously to calculate vertical heat advection-diffusion in the ice shelf. The initial condition for the second, numerical phase of the model is the profile obtained from our analytical solution (Eq. 7) at time  $t = T_o$ . The subglacial and oceanic tracer concentrations we assumed for the six chemical parameters are given in Table (1). We ran the two-phase analytical-numerical diffusion model for each chemical parameter separately, varying the amount of time during which the upper boundary condition reflected marine conditions and subglacial conditions ( $T_o$  and  $T_i$ ) from 1 to 10,000 years.

To determine which profiles fit the measured concentrations in the core, we compared the gradient of the top 0.5 m of each model run to the measured concentration profiles (Michaud et al., 2016a). We performed a least squares regression on the measured concentrations and tracked which model profiles fit within 95% confidence bounds for the measured values.

We also considered the possibility that vertical advection was occurring as groundwater flow, but were able to discount it based on considerations of the Peclet number:

$$Pe = \frac{uH}{D_{sed}}, \quad (4)$$



where  $H$  is the length of the core and  $u$  is the velocity. In order for advection to be dominant (i.e.  $Pe \geq 1$ ),  $u$  must be at least 0.011 m/yr. However, this is an order of magnitude greater than previous calculations of upward groundwater flux on the Whillans Ice Stream (Christoffersen et al., 2014).

### 2.3 Radiocarbon Measurements and Modelling

We re-evaluated the radiocarbon data from the Siple Coast of the WAIS presented in Kingslake et al. (2018) to estimate the timing of Holocene grounding line retreat and re-advance in this region. We focused on 11 subglacial till samples collected between 1989 and 2013, and 23 sediment samples collected below the Ross Ice Shelf in 1978 and 2015. Site locations are shown in Fig. 1 and include: SLW, the Whillans Ice Stream (WIS), KIS, BIS, the Whillans Grounding Zone (WGZ), and the Ross Ice Shelf Project (RISP). Details of the core collection, storage, and radiocarbon analysis are described in Kingslake et al. (2018). Apparent carbon ages inferred from the fraction of modern radiocarbon ( $F_m$ ) in the samples were presented in the extended data section of Kingslake et al. (2018). Kingslake et al. (2018) were careful to note that the apparent radiocarbon ages were meaningless due to the fact that the samples consisted of a mixture of young radiocarbon-bearing organic matter and re-worked radiocarbon-dead organic matter, which resulted in carbon ages that are much older than the actual age of the last exposure to radiocarbon inputs.

To better understand the sources of organic matter found in our sediment samples, we collected new data on carbon and nitrogen present in the samples: 17 samples collected from subglacial sites, 17 samples from sub-ice shelf sites, and 2 samples melted out from basal ice collected at a subglacial site. Total carbon (TC), total organic carbon (TOC), and total nitrogen (TN) measurements were performed at the University of California Santa Cruz Stable Isotope Laboratory. Samples for TOC and  $\delta^{13}\text{C}_{\text{org}}$  determination were decarbonated via direct acidification with sulfurous acid. All samples were dried prior to weighing for measurement. TC and TN were measured simultaneously by Dumas combustion using a CE Instruments NC2500 elemental analyzer coupled to a ThermoFinnigan Delta Plus XP isotope ratio mass spectrometer. TOC and  $\delta^{13}\text{C}_{\text{org}}$  were measured independently on the same instrumentation. All measurements were calculated relative to an in-house gelatin standard, which was extensively calibrated against international standard reference materials. Typical reproducibility ( $1\sigma$ ) of duplicate measurements is better than 0.1 wt%C, better than 0.01 wt%N, and better than 0.1 permil  $\delta^{13}\text{C}$ . Finally, total inorganic carbon (TIC) was calculated as the difference of TC and TOC. The TOC measurements for our field sites are shown in Fig. 2b, and all results for TOC, TC, TIC, C:N, and  $\delta^{13}\text{C}_{\text{org}}$  are presented in the Supplemental Material.

To estimate the timing of retreat and re-advance of the grounding line along the Whillans Ice Plain, we developed a two-phase model of  $^{14}\text{C}$  and  $^{12}\text{C}$  evolution at our field sites from 10,000 years ago to the present (see Fig. 3 schematic). We again used 10,000 years ago as the earliest possible time the grounding line could have retreated behind our field sites. The first model phase represented the time after grounding line retreat beyond the sediment sampling locations (Fig. 3). We assumed that at the onset of post-LGM grounding line retreat in the Ross Sea Sector, sediments at our field sites contained



190 no  $^{14}\text{C}$ , but did contain organic matter with  $^{12}\text{C}$  (Fig. 3). Given the short half-life of radiocarbon and the geologic evidence suggesting that the grounding line in the Ross Sea was at its LGM maximum position at roughly 30,000 years ago, we followed the conjecture of Kingslake et al. (2018) that  $^{14}\text{C}$  found in the sediments was incorporated after the post-LGM grounding line retreat. New,  $^{14}\text{C}$ -bearing marine organic matter was thus introduced into radiocarbon-free sediments during this first model phase (Fig. 3). We assumed a constant rate of  $^{14}\text{C}$  deposition,  $a$ , and a constant rate of  $^{12}\text{C}$  deposition,  $A$ , for  
195 the entire first phase of the model, when sediments were assumed to be exposed to input of radiocarbon-bearing marine organic matter. The ratio of  $^{14}\text{C}$  to  $^{12}\text{C}$  at the time of deposition was taken to be equal to that measured in modern amphipods collected at the grounding zone of the Whillans Ice Stream (WGZ) in 2015 (Kingslake et al., 2018). Because these amphipods were part of the marine food chain beneath the Ross Ice Shelf, we assumed that their  $Fm$  is representative of the  $Fm$  of the ocean water in the grounding line environment. The  $Fm$  for the amphipods corresponds to a radiocarbon reservoir age of ca. 1000 years for the sub-ice shelf marine organic matter. We represented the evolution of  $^{14}\text{C}$  concentration,  $n$ ,  
200 during this phase by accounting for both the addition and decay of  $^{14}\text{C}$ , with the equation:

$$n(t) = a\tau \left(1 - e^{-\frac{t}{\tau}}\right) \quad (5)$$

205 Where  $t$  is time and  $\tau$  is the mean lifetime of  $^{14}\text{C}$  (8033 years, based off the Libby half-life of  $^{14}\text{C}$  [Stuiver and Polach, 1977]). We represented the time-dependent concentration of  $^{12}\text{C}$  ( $N$ ) during the first model phase using the equation:

$$N(t) = N_o + At \quad (6)$$

210 Where  $N_o$  is the amount of  $^{12}\text{C}$  present initially in the system. We ran the first phase of the model from  $t = 0$  to  $t = T_o$ , where  $T_o$  is the length of time a given field site is exposed to the ocean. The second model phase represents the time after the ice sheet again covered a given site, and the only process affecting  $^{14}\text{C}$  concentration is radioactive decay (Fig. 3). We represented the  $^{14}\text{C}$  concentration with the equation:

$$215 \quad n(t) = n^* e^{-\frac{t}{\tau}} \quad (7)$$

Where  $n^*$  is the value of  $n$  when the system switches from sub-ice shelf to subglacial. After a site is glaciated, inputs of marine organic matter cease, and thus we took  $^{12}\text{C}$  to be constant with time at the value it had at the moment of grounding ( $N^*$ ):

$$220 \quad N(t) = N^* \quad (8)$$



Detailed derivation of these equations is shown in the Supplemental Material.

225 To normalize our results, we calculated TOC normalized to a 100g sample of dry sediments. We added  $n(t)$  and  $N(t)$  and divided by 100g of sediment. To calculate  $Fm$ , we divided  $n(t)$  by  $N(t)$ , and divided the quotient by the modern ratio of  $^{14}\text{C}$  to  $^{12}\text{C}$  ( $1.176 \times 10^{-12}$ ).

Organic carbon input to the sediments likely comes predominantly from local fecal pellets and necromass of macro, micro, and meiofauna, with a potential additional syndepositional regional input by sub-ice shelf water column advection. 230 During borehole drilling at WGZ, where the water column was only 10 m thick, higher than expected concentration of living biomass were observed in the form of planktic and nektonic organisms, including amphipods, fish, and jellies (whereas no multicellular life was noted at SLW). The only potential evidence noted of benthic organisms at WGZ was rare organic sheaths, presumably from infaunal meiofauna at the sediment-water interface. The absence of a developed benthic community is likely due to high sediment rainout from melt of debris-laden basal ice, as observed by borehole cameras. 235 Low concentrations of infauna were noted in the upper 10 cm at RISP (Harwood et al., 1989; Kellogg and Kellogg, 1981), ca. 100 km from WGZ, which is reflected in the relatively higher  $Fm$  measured in those samples. Although it is difficult to discern a sediment flux rate at WGZ from these observations, we were able to determine the accumulation of carbon in the sub-ice shelf ocean cavity by running the model for both RISP and WGZ, where we could ignore the re-advance of the grounding line (phase two of the model). Here, we expect them to be similar to the sub-ice shelf conditions experienced by 240 our field sites following grounding line retreat, i.e., in the first phase of the model. We thus ran phase one of the model for RISP and WGZ for  $t$  equaling  $10,000 \pm 2,000$  years. Because previous studies have placed the grounding line at Ross Island ca. 8000 years ago (Baroni and Hall, 2004; Licht et al., 1996; McKay et al., 2016), we set 8000 years ago as the latest the grounding line could have retreated beyond RISP and WGZ, and also examine the preceding 4000 years. For each model run we varied the value of  $A$  in increments of  $10^{-7}$  from  $10^{-7}$  to  $2 \times 10^{-5}$  and varied the value of  $N_o$  in increments of 0.0025 245 from 0 to 0.5. To test which values of  $A$  and  $N_o$  fit observations, we compared the  $Fm$  and TOC resulting from our calculations of  $^{14}\text{C}$  and  $^{12}\text{C}$  to measured values at WGZ and RISP and noted which values of  $A$  and  $N_o$  produced  $Fm$  and TOC values that fell within the maximum and minimum observed values. Values of  $A$  that fit the data ranged from  $4 \times 10^{-7}$  to  $1.24 \times 10^{-5}$  g/yr per 100 grams of dry sediment. The upper range of these values is comparable to the accumulation rate of organic carbon in modern Ross Sea sediments, of the order of  $10^{-5}$  g/yr per 100 grams of dry sediments (recalculated from 250 data in Demaster et al. [1992] and Frignani et al. [1998]).

With parameter ranges for  $a$  and  $A$  constrained using sample radiocarbon data from RISP, WGZ, and modern amphipods, we then ran the model for all subglacial cores for which radiocarbon has been measured. We varied  $A$  over the range determined from RISP and WGZ, varied  $N_o$  from 0.2g to 0.7g (normalized to a 100g sample of dry sediment), and varied the length of exposure to sub-ice shelf conditions as well as the time period of subsequent subglacial conditions from 255 0 to 10,000 years each. As with the model runs for RISP and WGZ, we checked whether each model run was compatible with our measurements by comparing the calculated  $Fm$  to the measured  $Fm$ . Although the samples were collected at the



260 same field sites in the same years,  $Fm$  and TOC could not be measured from the same sample; therefore, we tested whether modelled TOC fell within the maximum and minimum measurements of TOC for a given sampling location. Because we only had one measurement of TOC from BIS, we combined TOC measurements from BIS and KIS, and used maximum and minimum values of TOC as the bounds on TOC for both BIS and KIS. In our judgement, this approach is justified because values of  $Fm$  for both KIS and BIS are similar (Fig. 2a).

### 3 Results

#### 3.1 Ice Temperature Analysis

265 We used temperature modelling in ice to constrain the time since grounding line re-advance ( $T_i$ ) over the sites with steep observed basal temperature gradients (Fig. 4). We ran the model for  $0 \leq T_i \leq 10,000$  years, but because all basal temperature gradients  $\geq 50$  °C/km – the definition of cold-based ice used in Engelhardt (2004) – occur when  $T_i < 1700$  years, we only examine the model runs where  $0 \leq T_i \leq 2000$  years. Comparison of the observed basal temperature gradients to the model suggests that the grounding line advanced over KIS between  $\sim 1150$  and  $\sim 250$  years ago, over BIS between  $\sim 700$  and  $\sim 550$  years ago, and over UC between  $\sim 1500$  years and  $\sim 100$  years ago (Fig. 4). One basal temperature gradient measured for UC differs from the other two measurements noticeably (Fig. 4). This may be due to that location being separated from the others by a paleo-shear margin (named Fishhook) (Clarke et al., 2000). We account for vertical advection, but not horizontal advection in the temperature model. Because the Bindschadler Ice Stream is not currently stagnant and the Kamb Ice Stream has only been stagnant for the past ca. 150 years (Retzlaff and Bentley, 1993), temperature modelling cannot be used to determine a precise time since grounding, but rather it provides a more general idea of how long ago grounding occurred. Importantly, the only model runs that produced basal temperature gradients comparable to those measured at KIS, BIS, and UC were those that assumed ice grounding within the last 1500 years. The temperature modelling through ice also allows us to estimate basal ice thickness growth after grounding. The maximum thickness of basal ice for the three locations examined was 7.7 m for KIS, 5.4 m for BIS, and 8.9 m for UC. These thicknesses only account for the accretion of pure ice, and do not include the contribution of any incorporated debris to the total thickness of debris-laden ice. Given the simplicity of our model, these values are reasonably close to the thickness of debris-laden basal ice (ca. 10-20 m) observed in boreholes in this region (e.g., Christoffersen et al., 2010; Vogel et al., 2005).

#### 3.2 Ionic Diffusion Modelling

285 Ionic diffusion modelling of SLW allowed us to constrain  $T_i$  better than  $T_o$ . For each chemical parameter examined, the modelled diffusion profiles that fit the measured concentration profiles were in agreement with regards to exposure time to ocean ( $T_o$ ) and subglacial ( $T_i$ ) conditions (Fig. 5). We were able to fit diffusion profiles for every value of  $T_o$  tested, which impeded our ability to eliminate some lengths of  $T_o$  and therefore identify the length of time SLW was exposed to the ocean.



Conversely, we were successful in constraining the time since grounding line re-advance ( $T_i$ ) as the majority of the diffusion profiles that fit the measured porewater concentrations fall within the past 2300 years.

### 290 3.3 Radiocarbon Modelling

The  $F_m$  values reported in Kingslake et al. (2018) and used in this study spanned from  $0.0143 \pm 0.0004$  to  $0.1058 \pm 0.0013$  (Fig. 2a). Ocean cavity samples recovered from RISP and WGZ showed greater spread in values of  $F_m$  than those recovered from sites below grounded ice. Samples with  $F_m$  values closest to the modern reference  $^{14}\text{C}/^{12}\text{C}$  ratio were recovered from the sub-ice shelf cavity of the Ross Ice Shelf (RISP and WGZ), and samples furthest from the modern reference  $^{14}\text{C}/^{12}\text{C}$  ratio were recovered from below the Kamb and Bindschadler Ice Streams. Even the samples taken from the ocean cavity (i.e. WGZ and RISP) contain only 10% or less of radiocarbon compared to the modern standard. The carbon-to-nitrogen ratio (C:N) of the organic matter from the RISP samples is also the closest to the typical 6.7:1 ratio measured in the ocean (Redfield, 1958) (Fig. 9), suggesting a significant input of marine organic matter consistent with the exposure of this site to the seawater below the Ross Ice Shelf during the Holocene. The subglacial sediment samples have higher C:N ratios, from 15.4 – 49.4 (Table A1), which is consistent with their organic matter being a mixture of marine organic inputs and a pre-glacial, recalcitrant radiocarbon-dead component which originated from terrestrial plants (Fig. 9). The grounding zone deposits sampled at WGZ cluster between the subglacial and RISP samples in terms of their C:N ratios (Fig. 9). Excluding the C:N values from UC, Fig. 2c indicates that the C:N ratios increase with distance from the modern grounding line. The two UC sediment samples are considered outliers because they came from debris-laden ice (Vogel, 2004, p. 61) rather than from subglacial till. Hence, they retained low, marine-like, C:N ratios because the process of basal freeze-on incorporated sub-ice shelf sediments right after ice shelf re-grounding.

Surprisingly,  $F_m$  values for samples collected from sites currently in the ocean cavity differ only slightly from those currently located below grounded ice. For instance, the mean  $F_m$  of the eight SLW and WIS samples is  $0.050 \pm 0.006$  (standard error of the mean), while the corresponding mean and standard error for the six RISP samples is  $0.060 \pm 0.011$ . If the RISP samples were covered by ice today, it would take only  $\sim 1500$  years for their average  $F_m$  to drop to the level of the SLW/WIS samples through radioactive decay alone. The difference in  $F_m$  among all subglacial (SLW, WIS, KIS, and BIS) and sub-ice shelf samples (WGZ, RISP) is statistically insignificant based on the linear mixed-effects model (p-value of 0.141, intraclass correlation coefficient of 0.565). The two groups only become statistically independent of each other if we allow radioactive decay to occur in the samples below grounded ice for a period of at least an additional 1200 years.  $F_m$  values at KIS and BIS are similar to each other but differ from those at WIS and SLW (Fig. 2a), which are also similar to each other. The linear mixed-effects model indicates that KIS/BIS values are statistically independent of the WIS/SLW  $F_m$  values (p-value of  $2.11 \times 10^{-5}$ ). Overall, the sample-to-sample variations in  $F_m$  are relatively large compared to any variability due to differences in geographic settings of this sample population.



We used radiocarbon modelling to estimate the duration of ocean exposure following grounding line retreat ( $T_o$ ) and the time since ice shelf re-grounding ( $T_i$ ) (Fig. 6). Unfortunately, the radiocarbon modelling results are not very sensitive to  $T_i$  because the main process changing the simulated  $Fm$  of sediments after grounding is radiocarbon decay. That decay has a half-life of ca. 5000 years, or about half of the entire duration of the Holocene and much longer than values estimated for  $T_i$  through temperature or ionic diffusion modelling (0-2300 years for SLW, 100-1500 years for UC, 1150-250 years for KIS, and 550-700 years for BIS). Thus, we use the results from temperature and ionic diffusion modelling to constrain  $T_i$ .

325 Additionally, we use those ranges to further constrain the results of  $T_o$  found through radiocarbon modelling by only considering positive model outcomes where  $T_i$  falls within the range determined for each respective area. We then calculated the time of grounding line retreat by adding together  $T_o$  and  $T_i$  for each positive model run (Fig. 7). For WIS, where we could not perform ionic or temperature modelling to constrain  $T_i$ , we used results from the temperature modelling at UC, which is located only a few kilometers away, but across the current shear margin of Whillans Ice Stream. We combine the model results from every core at each site to estimate the peak of positive model outcomes for the timing of grounding line retreat at that site. For both KIS and BIS, the peak of positive model outcomes for the timing of grounding line retreat was ca. 2000 years ago (Fig. 8b). The positive model outcomes for SLW and WIS were more distributed, with peaks occurring at ca. 4000 and ca. 4500 years ago, respectively (Fig. 8b).

Radiocarbon modelling of the two cores from SLW produced slightly different results (Fig. 6). These differences may be attributed to the difference in coring methods employed and by the apparent heterogeneity in sediment  $Fm$ . The first core (SLW-PEC-1-34-35cm) was collected using a percussion corer, whereas the second (SLW-1 MC1B 0-8 bulk) was collected using a multicorer. The multicorer was designed to preserve and collect the surface sediments, whereas the percussion corer (which was acting as a gravity corer due to data communication issues) probably entered the sediment with backpressure in the barrel, thus blowing away soft surface sediments. Thus, the differences in  $Fm$  may result from the surface sediments being present in one core, but not the other. However, combining results from both cores indicates a peak in positive model outcomes for grounding line retreat at ca. 4000 years ago.

## 4 Discussion

### 4.1 Post-LGM Grounding Line Position

To cast our results in a regional context, we created a schematic diagram of grounding line positions in the Ross Embayment for the past 20,000 years (Fig. 8a). The grounding line along the flow line of the Bindschadler Ice Stream began retreating before 14,700 years ago and remained on the outer continental shelf until at least 11,500 years ago (Bart et al., 2018). The grounding line was then located at Roosevelt Island 3,200 years ago (Conway et al., 1999) before retreating beyond KIS and BIS ca. 2000 years ago; it then re-advanced over KIS and BIS ca. 500 years ago. The grounding line along the Transantarctic Mountain side of the Ross Embayment began retreating from its LGM position south of Coulman Island ca. 13,000 years ago (Anderson et al., 2014). This retreat was on average fairly rapid, as evidenced by the fact that the



grounding line reached WIS ca. 4500 years ago. The schematic for grounding line position along the Whillans Ice Stream flow line does not agree with all age constraints found in the Transantarctic Mountain Region (Fig. 8a). This could be because glaciers in the Transantarctic Mountains (for which the exposure ages were measured; Spector et al. [2017]) have a delayed response to grounding line retreat in the Ross Embayment, or because the grounding line retreated faster in the central Ross Embayment than along the sides. Grounding line re-advance also occurred relatively swiftly. Timing of this re-advance (ca. 1100 years ago for WIS and ca. 1000 years ago for SLW) is coincident with the grounding of Crary Ice Rise 1100 years ago (Bindschadler et al., 1990). Although Crary Ice Rise is significantly seaward of SLW, it is situated on a pronounced bathymetric high. Therefore, it is plausible that by grounding first, it provided backstress (Still et al., 2019), allowing ice thickening and slow-down to aid the process of grounding line re-advance for the Whillans Ice Stream (Fried et al., 2014).

#### 4.2 Ancillary Evidence Supporting Recent Grounding Line Re-advance

Our data analyses suggest that the modern configuration of grounding line positions in the study region has been attained relatively recently. This inference is consistent with the conspicuous absence of grounding zone wedges (GZWs) revealed by detailed seismic surveys at the mouth of the Kamb and Whillans Ice Streams (Horgan et al., 2013, 2017). These asymmetric sedimentary ridges can form quite rapidly during grounding zone stillstands. For instance, the height of the massive Whales Deep GZW in the eastern Ross Sea grew by about 0.1 m per year in the last ca. 1000 years of its formation after growing nearly an order of magnitude slower over the prior ca. 2000 years (Bart and Tulaczyk, 2020). Assuming this range of GZW growth rates of 0.01-0.1 m/yr, in one millennium of GZW stillstand, GZWs can achieve heights of 10-100m. GZWs of such height would be detectable with the active-source seismic methods employed by Horgan et al. (2013, 2017). Hence, the lack of seismic evidence for GZWs at the grounding zones of Kamb and Whillans Ice Streams corroborates the inference that the modern grounding line positions of these ice streams have not been attained until very recently.

The idea that the lower part of the Whillans Ice Stream grounded only recently is also consistent with attributes of the microbial ecosystem discovered in Subglacial Lake Whillans (Christner et al., 2014). Ammonium is the predominant dissolved inorganic nitrogen compound in the lake water column, which also hosts a high abundance of nitrifying microorganisms that obtain energy for chemosynthetic growth through oxidation of ammonia and nitrite (Christner et al., 2014). The source of ammonium for this community is diffusional flux from underlying sediment, facilitated by the activity of heterotrophic organisms which release ammonium via organic matter decomposition. While the abundant functional groups in the sediments shift to types associated with sulfur oxidation (Purcell et al., 2014) and methane oxidation (Michaud et al., 2016a) with depth, a diversity of heterotrophs exist in both the water and throughout the sediments sampled (Achberger et al., 2016). Similar phylotypes were also detected in sediments from KIS (Lanoil et al., 2009). Glacial meltwater contains no significant quantities of ammonia, and glacial erosion and grinding of minerals is not a significant source of nitrogen compounds (Tranter, 2014). Thus, a nitrifying microbial ecosystem in a subglacial lake, particularly one that is known to experience flushing of dissolved solutes (including nitrogen) from its lake waters every several years



(Tulaczyk et al., 2014; Vick-Majors et al., 2020), requires a significant source of bioavailable nitrogen. A recent advance of  
385 the ice sheet over sub-ice-shelf sediments like the ones sampled at RISP offers an attractive explanation for the subglacial  
source of nitrogen fueling the microbial ecosystem found in Subglacial Lake Whillans (e.g., Fig. 9). It is well established  
that decomposition in organic-poor marine sediments can yield extremely low C:N ratios due to retention of ammonia on  
clay particles accompanied by the escape of carbon dioxide formed during oxidation of organic carbon stored in sediments  
(e.g., Müller, 1977). Recent analyses of fluorophore components identified in fluorescent fractions of dissolved organic  
390 matter in SLW sediments, while not conclusive, support this notion, indicating characteristics of humic mixtures for coastal  
environments and marine sediments as well as Antarctic mountain glaciers and lakes (Vick-Majors et al., 2020). The  
ammonium-dominated, nitrifying microbial ecosystem of Subglacial Lake Whillans may, thus, be living off the legacy of  
marine organic matter stored in subglacial sediments for a relatively short period of time since the grounding line re-  
advanced over this region.

395 The mechanism described above also provides an explanation for the seemingly puzzling fact that the sub-ice shelf  
(RISP) sediment samples, which are exposed to seawater even now, have low C:N ratios, characteristic of marine sediments  
from a variety of locations (Müller, 1977), but have a very low *Fm* (0.06 on average). The RISP signature may be caused by  
the fact that much of the carbon, including radiocarbon, associated with young, recently produced organic matter, was part of  
labile organic molecules and hence, was preferentially digested during decomposition and released as carbon dioxide. This  
400 process, coupled with the fact that ammonia and ammonium are produced commonly in marine sediments through  
decomposition of marine organic matter rained out from the photic zone, can lower the C:N ratio of the sediments while  
removing some fraction of radiocarbon and leaving behind radiocarbon associated with more recalcitrant organic compounds  
which are radiocarbon-dead. The position of most subglacial sediment samples on the  $\delta^{13}\text{C}$  – C:N plot (Fig. 9) is consistent  
with the bulk of their organic matter originating from pre-glacial terrestrial C3 plants rich in recalcitrant components such as  
405 cellulose, lignin, or sporopollenin.

This interpretation is further corroborated by the fact that the two sediment samples from UC, which were melted  
out of basal ice rather than being sampled from beneath ice (Vogel, 2004, p. 61), show C:N ratios almost as low as those  
observed in the modern sub-ice shelf sediments of RISP and WGZ (Fig. 2c; Fig. 9). Microbial activity, including microbial  
consumption of nitrogen, is either nil or very slow in sediments incorporated into basal ice as compared to subglacial  
410 sediments (Montross et al., 2014). Thus, we interpret that UC's basal ice formed through freeze-on after ice shelf re-  
grounding took place in the Late Holocene, and that the freeze-on process incorporated sediments containing fresh organic  
marine matter with a low C:N ratio into the ice. Incidentally, this interpretation of observed low C:N ratios in the two  
sediment samples melted out from the basal ice of UC inspired our approach to modelling high basal temperature gradients  
resulting from recent ice shelf re-grounding.

415 Additionally, some evidence supporting recent grounding line re-advance has been reported in previous studies.  
Currently the Siple Coast ice streams are thickening (Joughin and Tulaczyk, 2002), which is consistent with ice sheet  
advance. Furthermore, the Siple Coast ice streams have experienced stagnation and reactivation in the past thousand years



(Catania et al., 2012), which could potentially be part of the ice shelf grounding process. After examining folds within the Ross Ice Shelf, Hulbe and Fahnestock (2007) concluded that the Whillans Ice Stream must have stopped flowing around 850  
420 years ago. However, we provide an alternative explanation for the folds in the ice layers by positing that they did not form as the ice stream slowed down, but rather as a result of ice shelf grounding. Evidence supporting recent floatation of the lower part of Kamb Ice Stream found by Catania et al, (2005, 2006) is consistent with the grounding line re-advancing to its modern position within the last few hundred years. Finally, very recent grounding of a thin ice shelf produces steep basal temperature gradients, which should result in a rapid basal freezing that may be responsible for the observed frozen-on basal  
425 layers found in KIS boreholes (Christoffersen et al., 2010; Vogel et al., 2005) and at WGZ (unpublished data).

### 4.3 Holocene Climate-Driven Grounding Line Fluctuations

There are varied ideas in the scientific literature as to the mechanisms causing the Holocene grounding line advance in the Ross Embayment. Kingslake et al. (2018) proposed that the grounding line re-advance was dominantly due to glacioisostatic rebound following unloading from ice sheet thinning and retreat. Lowry et al. (2019) suggest that this retreat  
430 is earlier than, and incompatible with, estimates of ice surface lowering in the Transantarctic Mountains as determined by exposure age dating. Here, we propose that both the grounding line retreat and re-advance is attributable to Holocene climate variability. The timing of grounding line retreat (re-advance) coincides with atmospheric warming (cooling) seen in the WAIS Divide ice core (Fig. 7) (Cuffey et al., 2016; Cuffey, 2017). Radiocarbon dating of elephant seal skins found on raised beaches along the Victoria Land Coast indicate two periods during the Holocene when ocean temperatures in this  
435 region were warm enough to suppress sea ice formation (Hall et al., 2006). The timing of the first warm period (6800 – 4500 years ago) corresponds reasonably well to the grounding line retreat over SLW and WIS, and the second (2300 – 1000 years ago) coincides with grounding line retreat over KIS and BIS. Following the most recent warm period, ocean temperatures cooled and sea ice cover expanded (Hall et al., 2006). The timing of this ocean cooling corresponds to the cooling period recorded in the WAIS Divide ice core and is remarkably consistent with our estimates of grounding line re-advance over all  
440 four subglacial sites (SLW, WIS, KIS, BIS). This suggests that the grounding line re-advance was caused by ocean cooling. This is in agreement with results from WAIS simulations indicating Holocene grounding line positions to be most sensitive to ocean temperatures (Lowry et al., 2019). The proposed high sensitivity of WAIS grounding line positions to relatively small Holocene climate variability may have implications for projections of grounding line behavior during the 21<sup>st</sup> Century as the temperature changes that coincided with the extensive Holocene grounding line retreat are on par with projections of  
445 temperature changes by the end of this century (Fig. 7) (Collins et al., 2013; Cuffey et al., 2016; Cuffey, 2017).

### 4.4 Revisiting the Unicorn Paradox

One puzzling observation noted by Engelhardt (2004) about observed basal temperature gradients from the Siple Coast was the difference in basal temperature gradients at UC and WIS. UC is completely surrounded by the Whillans Ice Stream, however, the basal temperature gradients measured at UC were much steeper than those measured a few kilometers



450 away at WIS. Engelhardt (2004) reasoned that cold ice at the bottom of UC could not have formed locally, but rather must  
have flowed there from Kamb Ice Stream during a proposed “super-surge” event. Given that the grounding line retreated  
beyond this area within the Holocene (Kingslake et al., 2018), we conjecture that the steep basal temperature gradient is  
instead a transient signal resulting from recent re-grounding of an ice shelf. If this is correct, Engelhardt’s super-surge event  
was simply due to this part of the ice sheet experiencing transient ungrounding and re-grounding as the grounding line first  
455 retreated upstream, and then subsequently re-advanced over the sites where Engelhardt measured ice temperature profiles.  
Temperature modelling from this study dates the grounding of UC to between ca. 1500 and ca. 100 years ago. This time  
frame broadly fits within the range of values of  $T_i$  found for WIS and SLW. The difference in basal temperature gradients  
between UC and WIS can be explained by the velocity of the ice. UC is frozen to the bed and has very low surface  
velocities. Contrarily, WIS has surface velocities of several hundred meters per year. Thus, the ice at the base of WIS  
460 reflects migration from upstream and does not record the thermal effects of the recent ice shelf re-grounding in the same way  
that the slow-moving ice column of UC still does.

## 5 Conclusions

In this study, we use several lines of evidence and seek to help refine the current understanding of grounding line  
activity in the Ross Sea after the LGM. Modelling of subglacial radiocarbon concentrations allows us to estimate the length  
465 of ocean exposure ( $T_o$ ) experienced by our field sites following grounding line retreat, and modelling of ice temperature and  
sediment porewater chemistry data enables us to assess the timing of grounding line re-advance ( $T_i$ ). Kingslake et al. (2018),  
who first proposed that the grounding line in the Siple Coast region retreated past its modern positions after the LGM,  
favored the explanation that their retreat resulted from a dynamic overshoot and their re-advance was driven by  
glacioisostatic rebound.

470 Here, we propose an alternative model whereby the grounding line retreated over our field sites as late as the mid-  
to late-Holocene and subsequently re-advanced during the late Holocene in response to climate cooling during the last 1000  
– 2000 years. Grounding line advance during the late Holocene occurred in spite of the fact that the WAIS Divide ice core  
shows a ~20% drop in ice accumulation rate over the past 2000 years, from a maximum reached around 4000 years B.P.  
(Buizert et al., 2015) – that is when our data suggest grounding line retreat. This counterintuitive relationship between ice  
475 input rates and grounding line motion places emphasis on ice-ocean interactions as the process capable of translating modest  
Holocene climate changes (corresponding to temperature variations of less than 2°C at WAIS Divide) to grounding line  
migration of hundreds of kilometers (Lowry et al., 2019). By suggesting strong climate sensitivity with regard to both retreat  
and advance, our hypothesis may raise further concern for accelerated future grounding line retreat with increasingly warmer  
sub-ice shelf oceanic input. We note that it is now recognized that at least some sections of the Greenland ice sheet retreated  
480 during the mid-Holocene climate optimum, and re-advanced during the late Holocene cooling (Vasskog et al., 2015).  
Further investigations into the relationship of these Antarctic and Greenland ice sheet fluctuations to Holocene climate



variability present an opportunity to reveal the sensitivity of these ice sheets to the slightly warmer climate states that may be reached in the very near future.

Our results are conjectural, largely because they are based on samples and measurements collected for other  
485 research reasons. However, our study highlights the value of maintaining archival materials because we were able to glean a  
greater understanding of grounding line movement in the Ross Sea by applying new modelling approaches to previously  
published data collected in different locations from multiple drilling projects over a period of more than 40 years. Future  
focused studies may be able to test our hypothesis. Similar efforts should also be aimed at other Antarctic ice sheet margins  
where it may be generally assumed that the grounding line was insensitive to Holocene climate variability, simply because  
490 no positive evidence has yet been collected. Insights into the response of Antarctic grounding lines to Holocene climate  
changes will inform projections of Antarctic ice sheet evolution under near-future climates, regardless of whether such  
insights will indicate high climate sensitivity or a general lack of climate sensitivity.

### Data Availability

With the exception of the TOC, C:N and  $\delta^{13}\text{C}$  measurements which are presented in the Supplemental Material, all data  
495 analyzed in this study has been previously published.

### Author Contribution

SN designed this research, performed analysis, and wrote the manuscript. ST co-designed this research, performed analysis,  
and contributed to the writing and editing of the manuscript. NS performed radiocarbon analysis. RS, RP, JC, and ST  
collected SLW and WGZ sediment samples and performed sedimentological analyses. ST, RP, JM, and RS wrote proposals  
500 that funded the collection of sediment samples from SLW and WGZ. NS, JC, RS, JM, and RP contributed to the writing and  
editing of the manuscript.

### Competing Interests

The authors declare that they have no conflict of interest.

### Acknowledgements

505 This research was supported by NSF grants: 0838947, 0839142, 1739027. Collection of SLW and WGZ sediment cores was  
supported by the U.S. National Science Foundation as part of the interdisciplinary WISSARD (Whillans Ice Stream  
Subglacial Access Research Drilling) project. The U.S. National Science Foundation also supported past drilling projects  
that enabled the collection of RISP, WIS, KIS, and BIS samples. The drilling team from University of Nebraska–Lincoln,



the WISSARD traverse personnel, the U.S. Antarctic Program, the New York Air National Guard, and Kenn Borek Air  
510 provided technical and logistical support. We are thankful to Ryan Venturelli and Brad Rosenheim for helpful discussions  
of radiocarbon analysis in Antarctic subglacial sediments. Statistical analysis was aided by John Neuhaus.

## References

- Achberger, A. M., Christner, B. C., Michaud, A. B., Priscu, J. C., Skidmore, M. L., Vick-Majors, T. J., Adkins, W.,  
Anandkrishnan, S., Barbante, C., Barcheck, G., Beem, L., Behar, A., Beitch, M., Bolsey, R., Branecky, C., Carter, S.,  
515 Christianson, K., Edwards, R., Fisher, A., Fricker, H., Foley, N., Guthrie, B., Hodson, T., Jacobel, R., Kelley, S., Mankoff,  
K., McBryan, E., Mikucki, J., Mitchell, A., Powell, R., Purcell, A., Sampson, D., Scherer, R., Sherve, J., Siegfried, M. and  
Tulaczyk, S.: Microbial community structure of subglacial Lake Whillans, West Antarctica, *Front. Microbiol.*, 7(SEP), 1–13,  
doi:10.3389/fmicb.2016.01457, 2016.
- Adkins, J. F. and Schrag, D. P.: Reconstructing Last Glacial Maximum bottom water salinities from deep-sea sediment pore  
520 fluid profiles, *Earth Planet. Sci. Lett.*, 216(1–2), 109–123, doi:10.1016/S0012-821X(03)00502-8, 2003.
- Anderson, J. B., Conway, H., Bart, P. J., Witus, A. E., Greenwood, S. L., McKay, R. M., Hall, B. L., Ackert, R. P., Licht, K.,  
Jakobsson, M. and Stone, J. O.: Ross Sea paleo-ice sheet drainage and deglacial history during and since the LGM, *Quat.*  
*Sci. Rev.*, 100, 31–54, doi:10.1016/j.quascirev.2013.08.020, 2014.
- Bamber, J. L., Oppenheimer, M., Kopp, R. E., Aspinall, W. P. and Cooke, R. M.: Ice sheet contributions to future sea-level  
525 rise from structured expert judgment, *Proc. Natl. Acad. Sci. U. S. A.*, 166(23), 11195–11200, doi:10.1073/pnas.1817205116,  
2019.
- Baroni, C. and Hall, B. L.: A new Holocene relative sea-level curve for Terra Nova Bay, Victoria Land, Antarctica, *J. Quat.*  
*Sci.*, 19(4), 377–396, doi:10.1002/jqs.825, 2004.
- Bart, P. J. and Tulaczyk, S.: A significant acceleration of ice volume discharge preceded a major retreat of a West Antarctic  
530 paleo-ice stream, *Geology*, 48(4), 313–317, doi:10.1130/G46916.1, 2020.
- Bart, P. J., DeCesare, M., Rosenheim, B. E., Majewski, W. and McGlannan, A.: A centuries-long delay between a paleo-ice-  
shelf collapse and grounding-line retreat in the Whales Deep Basin, eastern Ross Sea, Antarctica, *Sci. Rep.*, 8(1), 1–9,  
doi:10.1038/s41598-018-29911-8, 2018.
- Begeman, C. B., Tulaczyk, S. M., Marsh, O. J., Mikucki, J. A., Stanton, T. P., Hodson, T. O., Siegfried, M. R., Powell, R.  
535 D., Christianson, K. and King, M. A.: Ocean Stratification and Low Melt Rates at the Ross Ice Shelf Grounding Zone, *J.*  
*Geophys. Res. Ocean.*, 123(10), 7438–7452, doi:10.1029/2018JC013987, 2018.
- Bentley, M. J., Ocofaigh, C., Anderson, J. B., Conway, H., Davies, B., Graham, A. G. C., Hillenbrand, C. D., Hodgson, D.  
A., Jamieson, S. S. R., Larter, R. D., Mackintosh, A., Smith, J. A., Verleyen, E., Ackert, R. P., Bart, P. J., Berg, S.,  
Brunstein, D., Canals, M., Colhoun, E. A., Crosta, X., Dickens, W. A., Domack, E., Dowdeswell, J. A., Dunbar, R.,  
540 Ehrmann, W., Evans, J., Favier, V., Fink, D., Fogwill, C. J., Glasser, N. F., Gohl, K., Gollgede, N. R., Goodwin, I., Gore, D.



- B., Greenwood, S. L., Hall, B. L., Hall, K., Hedding, D. W., Hein, A. S., Hocking, E. P., Jakobsson, M., Johnson, J. S., Jomelli, V., Jones, R. S., Klages, J. P., Kristoffersen, Y., Kuhn, G., Leventer, A., Licht, K., Lilly, K., Lindow, J., Livingstone, S. J., Massé, G., McGlone, M. S., McKay, R. M., Melles, M., Miura, H., Mulvaney, R., Nel, W., Nitsche, F. O., O'Brien, P. E., Post, A. L., Roberts, S. J., Saunders, K. M., Selkirk, P. M., Simms, A. R., Spiegel, C., Stollendorf, T. D.,  
545 Sugden, D. E., van der Putten, N., van Ommen, T., Verfaillie, D., Vyverman, W., Wagner, B., White, D. A., Witus, A. E. and Zwartz, D.: A community-based geological reconstruction of Antarctic Ice Sheet deglaciation since the Last Glacial Maximum, *Quat. Sci. Rev.*, 100, 1–9, doi:10.1016/j.quascirev.2014.06.025, 2014.
- Bindschadler, R. A., Roberts, E. P. and Iken, A.: Age of Cray Ice Rise, Antarctica, determined from temperature-depth profiles, *Ann. Glaciol.*, 14, 13–16, 1990.
- 550 Boudreau, B. P.: The diffusive tortuosity of fine-grained unlithified sediments, *Geochim. Cosmochim. Acta*, 60(16), 3139–3142, doi:10.1016/0016-7037(96)00158-5, 1996.
- Bradley, S. L., Hindmarsh, R. C. A., Whitehouse, P. L., Bentley, M. J. and King, M. A.: Low post-glacial rebound rates in the Weddell Sea due to Late Holocene ice-sheet readvance, *Earth Planet. Sci. Lett.*, 413, 79–89, doi:10.1016/j.epsl.2014.12.039, 2015.
- 555 Buizert, C., Cuffey, K. M., Severinghaus, J. P., Baggenstos, D., Fudge, T. J., Steig, E. J., Markle, B. R., Winstrup, M., Rhodes, R. H., Brook, E. J., Sowers, T. A., Clow, G. D., Cheng, H., Edwards, R. L., Sigl, M., McConnell, J. R. and Taylor, K. C.: The WAIS Divide deep ice core WD2014 chronology &ndash; Part 1: Methane synchronization (68–31 ka BP) and the gas age-ice age difference, *Clim. Past*, 11(2), 153–173, doi:10.5194/cp-11-153-2015, 2015.
- Catania, G., Hulbe, C., Conway, H., Scambos, T. A. and Raymond, C. F.: Variability in the mass flux of the Ross ice  
560 streams, West Antarctica, over the last millennium, *J. Glaciol.*, 58(210), 741–752, doi:10.3189/2012JoG11J219, 2012.
- Catania, G. A., Conway, H., Raymond, C. F. and Scambos, T. A.: Surface morphology and internal layer stratigraphy in the downstream end of Kamb Ice Stream, West Antarctica, *J. Glaciol.*, 51(174), 423–431, doi:10.3189/172756505781829142, 2005.
- Catania, G. A., Conway, H., Raymond, C. F. and Scambos, T. A.: Evidence for floatation or near floatation in the mouth of  
565 Kamb Ice Stream, West Antarctica, prior to stagnation, *J. Geophys. Res. Earth Surf.*, 111(1), 1–10, doi:10.1029/2005JF000355, 2006.
- Christner, B. C., Priscu, J. C., Achberger, A. M., Barbante, C., Carter, S. P., Christianson, K., Michaud, A. B., Mikucki, J. A., Mitchell, A. C., Skidmore, M. L., Vick-Majors, T. J., Adkins, W. P., Anandkrishnan, S., Anandkrishnan, S., Beem, L., Behar, A., Beitch, M., Bolsey, R., Branecky, C., Fisher, A., Foley, N., Mankoff, K. D., Sampson, D., Tulaczyk, S., Edwards,  
570 R., Kelley, S., Sherve, J., Fricker, H. A., Siegfried, S., Guthrie, B., Hodson, T., Powell, R., Scherer, R., Horgan, H., Jacobel, R., McBryan, E. and Purcell, A.: A microbial ecosystem beneath the West Antarctic ice sheet, *Nature*, 512(7514), 310–313, doi:10.1038/nature13667, 2014.
- Christoffersen, P., Tulaczyk, S. and Behar, A.: Basal ice sequences in Antarctic ice stream: Exposure of past hydrologic conditions and a principal mode of sediment transfer, *J. Geophys. Res. Earth Surf.*, 115(3), 1–12,



- 575 doi:10.1029/2009JF001430, 2010.
- Christoffersen, P., Bougamont, M., Carter, S. P., Fricker, H. A. and Tulaczyk, S.: Significant groundwater contribution to Antarctic ice streams hydrologic budget, *Geophys. Res. Lett.*, 41(6), 2003–2010, 2014.
- Clark, P. U., Dyke, A. S., Shakun, J. D., Carlson, A. E., Clark, J., Wohlfarth, B., Mitrovica, J. X., Hostetler, S. W. and McCabe, A. M.: The Last Glacial Maximum, *Science* (80-. ), 325(5941), 710–714, doi:10.1126/science.1172873, 2009.
- 580 Clarke, T. S., Liu, C., Lord, N. E. and Bentley, C. R.: Evidence for a recently abandoned shear margin adjacent to ice stream B2, Antarctica, from ice-penetrating radar measurements, *J. Geophys. Res. Solid Earth*, 105(B6), 13409–13422, doi:10.1029/2000jb900037, 2000.
- Conway, H., Hall, B. L., Denton, G. H., Gades, A. M. and Waddington, E. D.: Past and future grounding-line retreat of the West Antarctic Ice Sheet, *Science* (80-. ), 286(5438), 280–283, doi:10.1126/science.286.5438.280, 1999.
- 585 Cuffey, K. M., Clow, G. D., Steig, E. J., Buizert, C., Fudge, T. J., Koutnik, M., Waddington, E. D., Alley, R. B. and Severinghaus, J. P.: Deglacial temperature history of West Antarctica, *Proc. Natl. Acad. Sci. U. S. A.*, 113(50), 14249–14254, doi:10.1073/pnas.1609132113, 2016.
- Cunningham, W. L., Leventer, A., Andrews, J. T., Jennings, A. E. and Licht, K. J.: Late Pleistocene-Holocene marine conditions in the Ross Sea, Antarctica: Evidence from the diatom record, *Holocene*, 9(2), 129–139, doi:10.1191/095968399675624796, 1999.
- 590 Demaster, D. J., Dunbar, R. B., Gordon, L. I., Leventer, A. R., Morrison, J. M., Nelson, D. M., Nittrouer, C. A. and Smith, W. O.: Cycling and accumulation of biogenic silica and organic matter in high-latitude environments: the Ross Sea, *Oceanography*, 5(3), 146–153, doi:10.5670/oceanog.1992.03, 1992.
- Engelhardt, H.: Thermal regime and dynamics of the West Antarctic ice sheet, *Ann. Glaciol.*, 39, 85–92, 2004.
- 595 Engelhardt, H. and Kamb, B.: Vertical temperature profile of Ice Stream B, *Antarct. JUS*, 28(5), 63–66, 1993.
- Engelhardt, H., Humphrey, N., Kamb, B. and Fahnestock, M.: Physical conditions at the base of a fast moving Antarctic ice stream, *Science* (80-. ), 248(4951), 57–59, doi:10.1126/science.248.4951.57, 1990.
- Fisher, A. T., Mankoff, K. D., Tulaczyk, S. M., Tyler, S. W. and Foley, N.: High geothermal heat flux measured below the West Antarctic Ice Sheet, *Sci. Adv.*, 1(6), e1500093–e1500093, doi:10.1126/sciadv.1500093, 2015.
- 600 Fretwell, P., Pritchard, H. D., Vaughan, D. G., Bamber, J. L., Barrand, N. E., Bell, R., Bianchi, C., Bingham, R. G., Blankenship, D. D., Casassa, G., Catania, G., Callens, D., Conway, H., Cook, A. J., Corr, H. F. J., Damaske, D., Damm, V., Ferraccioli, F., Forsberg, R., Fujita, S., Gim, Y., Gogineni, P., Griggs, J. A., Hindmarsh, R. C. A., Holmlund, P., Holt, J. W., Jacobel, R. W., Jenkins, A., Jokat, W., Jordan, T., King, E. C., Kohler, J., Krabill, W., Riger-Kusk, M., Langley, K. A., Leitchenkov, G., Leuschen, C., Luyendyk, B. P., Matsuoka, K., Mouginit, J., Nitsche, F. O., Nogi, Y., Nost, O. A., Popov, S. V., Rignot, E., Ripplin, D. M., Rivera, A., Roberts, J., Ross, N., Siegert, M. J., Smith, A. M., Steinhage, D., Studinger, M., Sun, B., Tinto, B. K., Welch, B. C., Wilson, D., Young, D. A., Xiangbin, C. and Zirizzotti, A.: Bedmap2: Improved ice bed, surface and thickness datasets for Antarctica, *Cryosphere*, 7, 375–393, doi:10.5194/tc-7-375-2013, 2013.
- 605 Fried, M. J., Hulbe, C. L. and Fahnestock, M. A.: Grounding-line dynamics and margin lakes, *Ann. Glaciol.*, 55(66), 87–96,



- doi:10.3189/2014AoG66A216, 2014.
- 610 Frignani, M., Giglio, F., Langone, L., Ravaioli, M. and Mangini, A.: Late Pleistocene-Holocene sedimentary fluxes of organic carbon and biogenic silica in the northwestern Ross Sea, Antarctica, *Ann. Glaciol.*, 27, 697–703, doi:10.3189/1998aog27-1-697-703, 1998.
- Hall, B. L., Hoelzel, A. R., Baroni, C., Denton, G. H., Le Boeuf, B. J., Overturf, B. and Töpf, A. L.: Holocene elephant seal distribution implies warmer-than-present climate in the Ross Sea, *Proc. Natl. Acad. Sci. U. S. A.*, 103(27), 10213–10217, doi:10.1073/pnas.0604002103, 2006.
- 615 Hall, B. L., Denton, G. H., Stone, J. O. and Conway, H.: History of the grounded ice sheet in the Ross Sea sector of Antarctica during the Last Glacial Maximum and the last termination, *Geol. Soc. London, Spec. Publ.*, 381(1), 167–181, doi:10.1144/SP381.5, 2013.
- Harwood, D. M., Scherer, R. P. and Webb, P. N.: Multiple Miocene marine productivity events in West Antarctica as recorded in upper Miocene sediments beneath the Ross Ice Shelf (Site J-9), *Mar. Micropaleontol.*, 15(1–2), 1–9, doi:10.1016/0377-8398(89)90006-6, 1989.
- 620 Horgan, H. J., Christianson, K., Jacobel, R. W., Anandakrishnan, S. and Alley, R. B.: Sediment deposition at the modern grounding zone of Whillans Ice Stream, West Antarctica, *Geophys. Res. Lett.*, 40(15), 3934–3939, doi:10.1002/grl.50712, 2013.
- 625 Horgan, H. J., Hulbe, C., Alley, R. B., Anandakrishnan, S., Goodsell, B., Taylor-Offord, S. and Vaughan, M. J.: Poststagnation Retreat of Kamb Ice Stream’s Grounding Zone, *Geophys. Res. Lett.*, 44(19), 9815–9822, doi:10.1002/2017GL074986, 2017.
- Hulbe, C. and Fahnestock, M.: Century-scale discharge stagnation and reactivation of the Ross ice streams, West Antarctica, *J. Geophys. Res. Earth Surf.*, 112(F03S27), doi:10.1029/2006JF000603, 2007.
- 630 Jones, R. S., Mackintosh, A. N., Norton, K. P., Golledge, N. R., Fogwill, C. J., Kubik, P. W., Christl, M. and Greenwood, S. L.: Rapid Holocene thinning of an East Antarctic outlet glacier driven by marine ice sheet instability, *Nat. Commun.*, 6, doi:10.1038/ncomms9910, 2015.
- Joughin, I. and Tulaczyk, S.: Positive mass balance of the Ross Ice Streams, West Antarctica, *Science* (80-. ), 295(5554), 476–480, doi:10.1126/science.1066875, 2002.
- 635 Kamb, B.: Basal zone of the West Antarctic ice streams and its role in lubrication of their rapid motion, in *Antarctic Research Series*, vol. 77, pp. 157–199., 2001.
- Kellogg, T. B. and Kellogg, D. E.: Pleistocene sediments beneath the Ross Ice Shelf, *Nature*, 293(5828), 130–133, doi:10.1038/293130a0, 1981.
- Kingslake, J., Scherer, R. P., Albrecht, T., Coenen, J., Powell, R. D., Reese, R., Stansell, N. D., Tulaczyk, S., Wearing, M. G. and Whitehouse, P. L.: Extensive retreat and re-advance of the West Antarctic Ice Sheet during the Holocene, *Nature*, 558(7710), 430–434, doi:10.1038/s41586-018-0208-x, 2018.
- 640 Lamb, A. L., Wilson, G. P. and Leng, M. J.: A review of coastal palaeoclimate and relative sea-level reconstructions using



- $\delta^{13}\text{C}$  and C/N ratios in organic material, *Earth-Science Rev.*, 75(1–4), 29–57, doi:10.1016/j.earscirev.2005.10.003, 2006.
- Lanoil, B., Skidmore, M., Priscu, J. C., Han, S., Foo, W., Vogel, S. W., Tulaczyk, S. and Engelhardt, H.: Bacteria beneath  
645 the West Antarctic Ice Sheet, *Environ. Microbiol.*, 11(3), 609–615, doi:10.1111/j.1462-2920.2008.01831.x, 2009.
- Lee, J. Il, McKay, R. M., Golledge, N. R., Yoon, H. Il, Yoo, K. C., Kim, H. J. and Hong, J. K.: Widespread persistence of  
expanded East Antarctic glaciers in the southwest Ross Sea during the last deglaciation, *Geology*, 45(5), 403–406,  
doi:10.1130/G38715.1, 2017.
- Li, Y.-H. and Gregory, S.: Diffusion of ions in sea water and in deep-sea sediments. *Geochim. Cosmochim. Acta*, *Geochim.*  
650 *Cosmochim. Acta*, 38(5), 703–714, doi:10.1016/0016-7037(74)90145-8, 1974.
- Licht, K. J., Jennings, A. E., Andrews, J. T. and Williams, K. M.: Chronology of late Wisconsin ice retreat from the western  
Ross Sea, Antarctica, *Geology*, 24(3), 223–226, doi:10.1130/0091-7613(1996)024<0223:COLWIR>2.3.CO;2, 1996.
- Licht, K. J., Hennessy, A. J. and Welke, B. M.: The U-Pb detrital zircon signature of West Antarctic ice stream tills in the  
Ross embayment, with implications for Last Glacial Maximum ice flow reconstructions, *Antarct. Sci.*, 26(6), 687–697,  
655 doi:10.1017/S0954102014000315, 2014.
- Lowry, D. P., Golledge, N. R., Bertler, N. A. N., Jones, R. S. and McKay, R.: Deglacial grounding-line retreat in the Ross  
Embayment, Antarctica, controlled by ocean and atmosphere forcing, *Sci. Adv.*, 5(8), doi:10.1126/sciadv.aav8754, 2019.
- McKay, R., Golledge, N. R., Maas, S., Naish, T., Levy, R., Dunbar, G. and Kuhn, G.: Antarctic marine ice-sheet retreat in  
the Ross Sea during the early Holocene, *Geology*, 44(1), 7–10, doi:10.1130/G37315.1, 2016.
- 660 Michaud, A. B., Skidmore, M. L., Mitchell, A. C., Vick-Majors, T. J., Barbante, C., Turetta, C., Van Gelder, W. and Priscu,  
J. C.: Solute sources and geochemical processes in Subglacial Lake Whillans, West Antarctica, *Geology*, 44(5), 347–350,  
doi:10.1130/G37639.1, 2016a.
- Michaud, A. B., Skidmore, M. L., Mitchell, A. C., Vick-Majors, T. J., Barbante, C., Turetta, C., VanGelder, W. and Priscu,  
J. C.: Supplemental material: Solute sources and geochemical processes in Subglacial Lake Whillans, West Antarctica, *Geol.*  
665 *Soc. Am.*, doi:10.1130/2016110, 2016b.
- Montross, S., Skidmore, M., Christner, B., Samyn, D., Tison, J. L., Lorrain, R., Doyle, S. and Fitzsimons, S.: Debris-Rich  
Basal Ice as a Microbial Habitat, Taylor Glacier, Antarctica, *Geomicrobiol. J.*, 31(1), 76–81,  
doi:10.1080/01490451.2013.811316, 2014.
- Müller, P. J.: C N ratios in Pacific deep-sea sediments: Effect of inorganic ammonium and organic nitrogen compounds  
670 sorbed by clays, *Geochim. Cosmochim. Acta*, 41(6), 765–776, doi:10.1016/0016-7037(77)90047-3, 1977.
- Purcell, A. M., Mikucki, J. A., Achberger, A. M., Alekhina, I. A., Barbante, C., Christner, B. C., Ghosh, D., Michaud, A. B.,  
Mitchell, A. C., Priscu, J. C., Scherer, R., Skidmore, M. L., Vick-Majors, T. J., Adkins, W. P., Anandakrishnan, S.,  
Barcheck, G., Beem, L., Behar, A., Beitch, M., Bolsey, R., Branecky, C., Carter, S., Christianson, K., Edwards, R., Fisher,  
A., Fricker, H., Foley, N., Guthrie, B., Hodson, T., Jacobel, R., Kelley, S., Mankoff, K., McBryan, E., Powell, R., Sampson,  
675 D., Severinghaus, J., Sherve, J., Siegfried, M. and Tulaczyk, S.: Microbial sulfur transformations in sediments from  
Subglacial Lake Whillans, *Front. Microbiol.*, 5(NOV), 1–16, doi:10.3389/fmicb.2014.00594, 2014.



- Redfield, A. C.: The biological control of chemical factors in the environment, *Am. Sci.*, 46(3), 230A, 205–221, 1958.
- Retzlaff, R. and Bentley, C. R.: Timing of stagnation of ice stream C, West Antarctica, from short-pulse radar studies of buried surface crevasses, *J. Glaciol.*, 39(133), 553–561, doi:10.1017/S0022143000016440, 1993.
- 680 Scherer, R. P., Aldahan, A., Tulaczyk, S., Possnert, G., Engelhardt, H. and Kamb, B.: Pleistocene collapse of the West Antarctic ice sheet, *Science* (80-. ), 281(5373), 82–85, doi:10.1126/science.281.5373.82, 1998.
- Spector, P., Stone, J., Cowderly, S. G., Hall, B., Conway, H. and Bromley, G.: Rapid early-Holocene deglaciation in the Ross Sea, Antarctica, *Geophys. Res. Lett.*, 44(15), 7817–7825, doi:10.1002/2017GL074216, 2017.
- Still, H., Campbell, A. and Hulbe, C.: Mechanical analysis of pinning points in the Ross Ice Shelf, Antarctica, *Ann. Glaciol.*,  
685 60(78), 32–41, doi:10.1017/aog.2018.31, 2019.
- Stuiver, M. and Polach, H. A.: Discussion Reporting of 14 C Data, *Radiocarbon*, 19(3), 355–363, doi:10.1017/S0033822200003672, 1977.
- Tranter, M.: Microbes eat rock under ice, *Nature*, 512(7514), 256–257, doi:10.1038/512256a, 2014.
- Tulaczyk, S., Kamb, B., Scherer, R. P. and Engelhardt, H. F.: Sedimentary processes at the base of a West Antarctic ice  
690 stream; constraints from textural and compositional properties of subglacial debris, *J. Sediment. Res.*, 68(3), 487–496, doi:10.2110/jsr.68.487, 1998.
- Tulaczyk, S., Kamb, B. and Engelhardt, H. F.: Estimates of effective stress beneath a modern West Antarctic ice stream from till preconsolidation and void ratio, *Boreas*, 30(2), 101–114, doi:10.1111/j.1502-3885.2001.tb01216.x, 2001.
- Tulaczyk, S., Mikucki, J. A., Siegfried, M. R., Priscu, J. C., Barcheck, C. G., Beem, L. H., Behar, A., Burnett, J., Christner, B. C., Fisher, A. T., Fricker, H. A., Mankoff, K. D., Powell, R. D., Rack, F., Sampson, D., Scherer, R. P. and Schwartz, S.  
695 Y.: WISSARD at Subglacial Lake Whillans, West Antarctica: scientific operations and initial observations, *Ann. Glaciol.*, 55(65), 51–58, doi:10.3189/2014aog65a009, 2014.
- Turcotte, D. and Schubert, G.: *Geodynamics*, 3rd ed., Cambridge University Press, Cambridge., 2014.
- Vasskog, K., Langebroek, P. M., Andrews, J. T., Nilsen, J. E. Ø. and Nesje, A.: The Greenland Ice Sheet during the last  
700 glacial cycle: Current ice loss and contribution to sea-level rise from a palaeoclimatic perspective, *Earth-Science Rev.*, 150, 45–67, doi:10.1016/j.earscirev.2015.07.006, 2015.
- Venturelli, R. A., Siegfried, M. R., Roush, K. A., Li, W., Burnett, J., Zook, R., Fricker, H. A., Priscu, J. C., Leventer, A. and Rosenheim, B. E.: Mid-Holocene Grounding Line Retreat and Readvance at Whillans Ice Stream, West Antarctica, *Geophys. Res. Lett.*, 47(15), doi:10.1029/2020GL088476, 2020.
- 705 Vick-Majors, T. J., Michaud, A. B., Skidmore, M. L., Turetta, C., Barbante, C., Christner, B. C., Dore, J. E., Christianson, K., Mitchell, A. C., Achberger, A. M., Mikucki, J. A. and Priscu, J. C.: Biogeochemical Connectivity Between Freshwater Ecosystems beneath the West Antarctic Ice Sheet and the Sub-Ice Marine Environment, *Global Biogeochem. Cycles*, 34(3), no, doi:10.1029/2019GB006446, 2020.
- Vogel, S.W.: The basal regime of the West-Antarctic ice sheet interaction of subglacial geology with ice dynamics, Ph.D.  
710 dissertation, University of California, Santa Cruz, 137 pp., 2004.

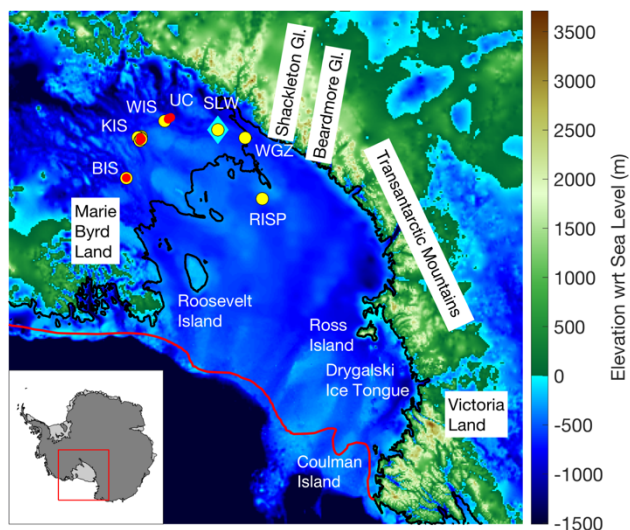


Vogel, S. W., Tulaczyk, S., Kamb, B., Engelhardt, H., Carsey, F. D., Behar, A. E., Lane, A. L. and Joughin, I.: Subglacial conditions during and after stoppage of an Antarctic Ice Stream: Is reactivation imminent?, *Geophys. Res. Lett.*, 32(14), 1–4, doi:10.1029/2005GL022563, 2005.

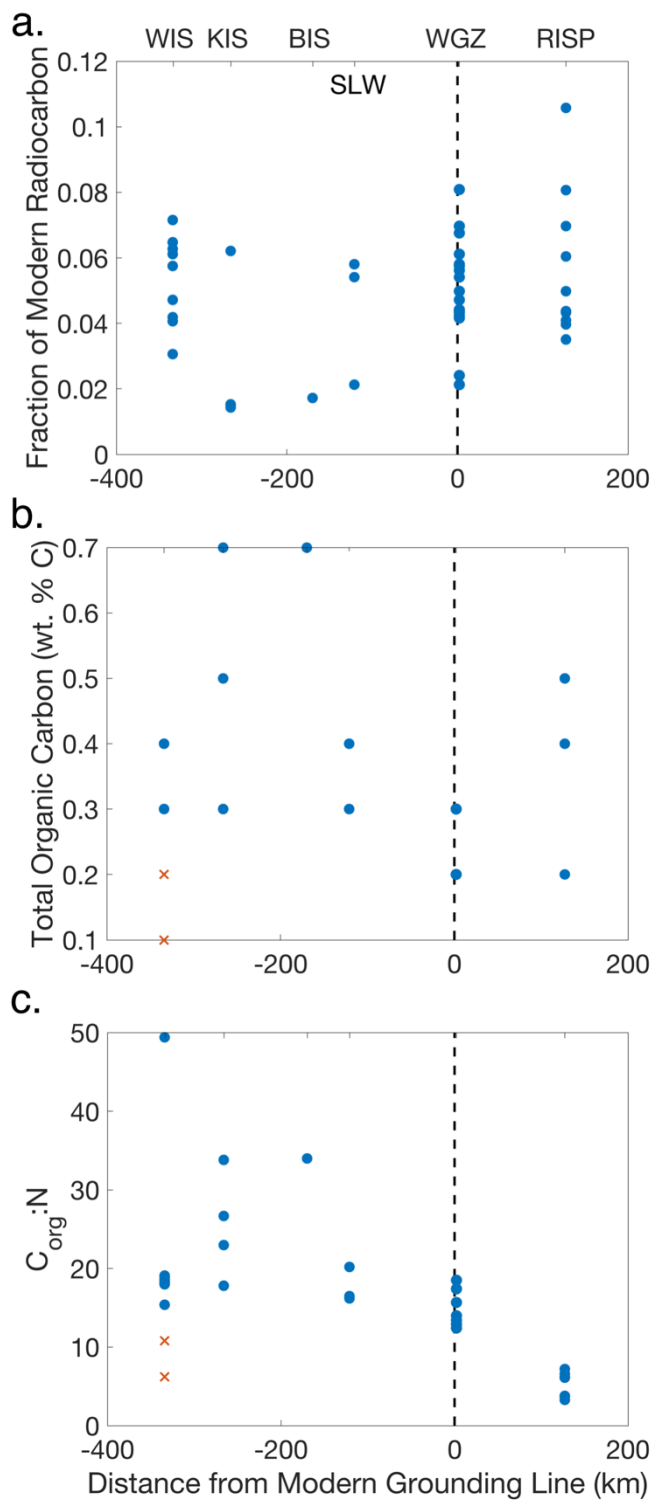
715 Waddington, E. D., Conway, H., Steig, E. J., Alley, R. B., Brook, E. J., Taylor, K. C. and White, J. W. C.: Decoding the dipstick: Thickness of Siple Dome, West Antarctica, at the Last Glacial Maximum, *Geology*, 33(4), 281–284, doi:10.1130/G21165.1, 2005.

Wang, J. H.: Self-Diffusion and Structure of Liquid Water. I. Measurement of Self-Diffusion of Liquid Water with Deuterium as Tracer, *J. Am. Chem. Soc.*, 73(2), 510–513, doi:10.1021/ja01146a002, 1951a.

720 Wang, J. H.: Self-diffusion and Structure of Liquid Water. II. Measurement of Self-diffusion of Liquid Water with O18 as Tracer, , 73(9), 4181–4183, doi:10.1021/ja01153a039, 1951b.



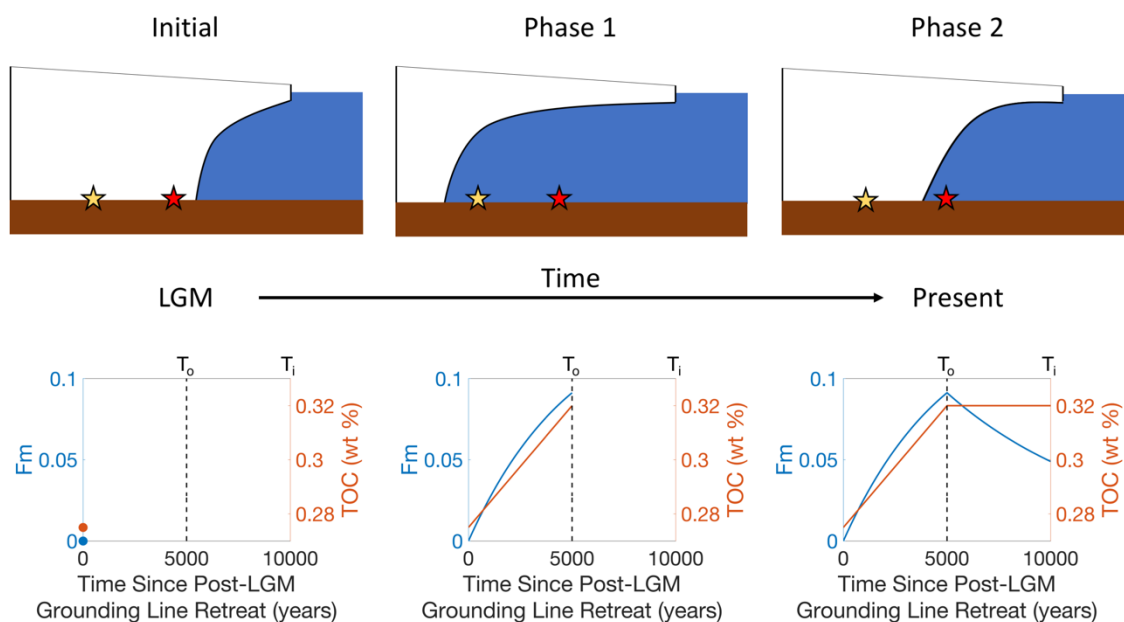
725 **Figure 1: Location of sites and place names used in this study. Background image uses bed elevation data (Fretwell et al., 2013). Yellow dots denote the location of sediment cores taken for radiocarbon and organic matter analyses. Red dots denote the location of deep ice-temperature profiles examined in this study. Cyan diamond indicates the location where sediment porewater was collected and analyzed.**





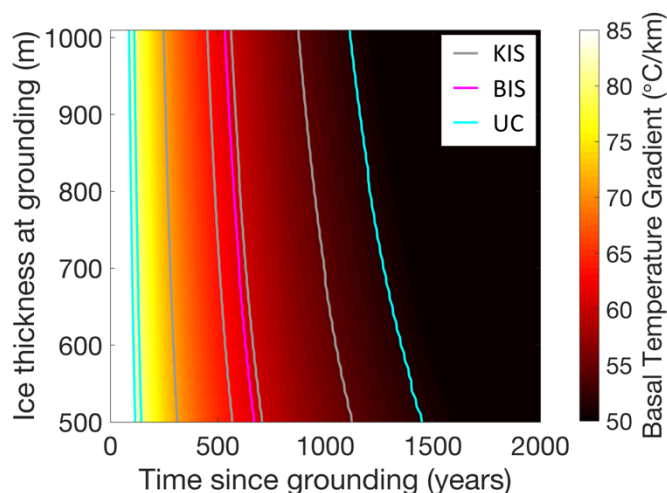
730 **Figure 2: Results of radiocarbon and organic matter analyses for sediment samples taken from beneath grounded ice (SLW, WIS, KIS, BIS), or beneath floating ice (RISP, WGZ), or entrained in basal ice (UC) plotted against sample position with respect to the modern grounding line. (a) Fraction of modern radiocarbon ( $F_m$ ) measured in acid-insoluble organic matter of from bulk sediments. (b) Total organic carbon (TOC). (c)  $C_{org}:N_{org}$  (atom:atom). Orange x's represent the values for sediments recovered from UC basal ice.**

735



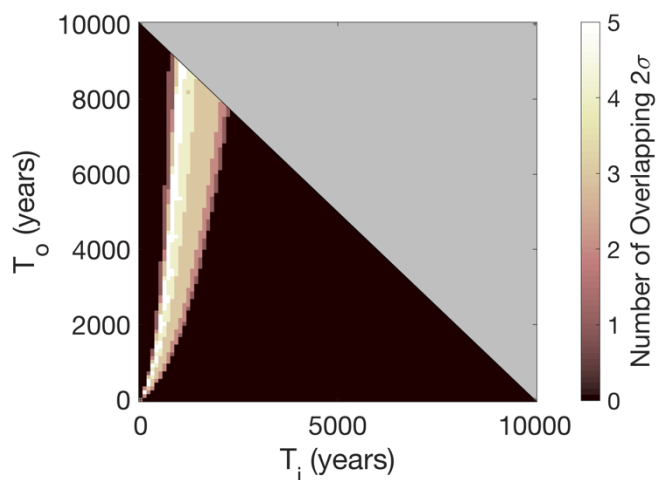
740

**Figure 3: Schematic of the two-phase model of radiocarbon evolution since onset of LGM grounding line retreat over the field sites. The yellow star represents subglacial field sites, whereas the red star represents sub-ice shelf sites. The evolutions of  $F_m$  and TOC are shown for subglacial field sites. For this run, both  $T_0$  and  $T_i$  equal 5000 years; the horizontal axis represents time since post-LGM grounding line retreat past a subglacial site (yellow star). Ocean exposure (when the grounding line had retreated beyond a site) begins at  $t = 0$  and is assumed here to last until  $t = 5000$  years. Subsequent grounding line re-advance occurs at  $t = 5000$  years and lasts until the end of the model run ( $t = 10,000$  years). Accumulation rates for  $^{14}C$  and  $^{12}C$  were assumed to be  $9.23 \times 10^{-18}$  g/yr and  $9.0 \times 10^{-6}$  g/yr per 100 grams of dry sediments, respectively. Note that the right-hand side axis (TOC) does not start at zero.**



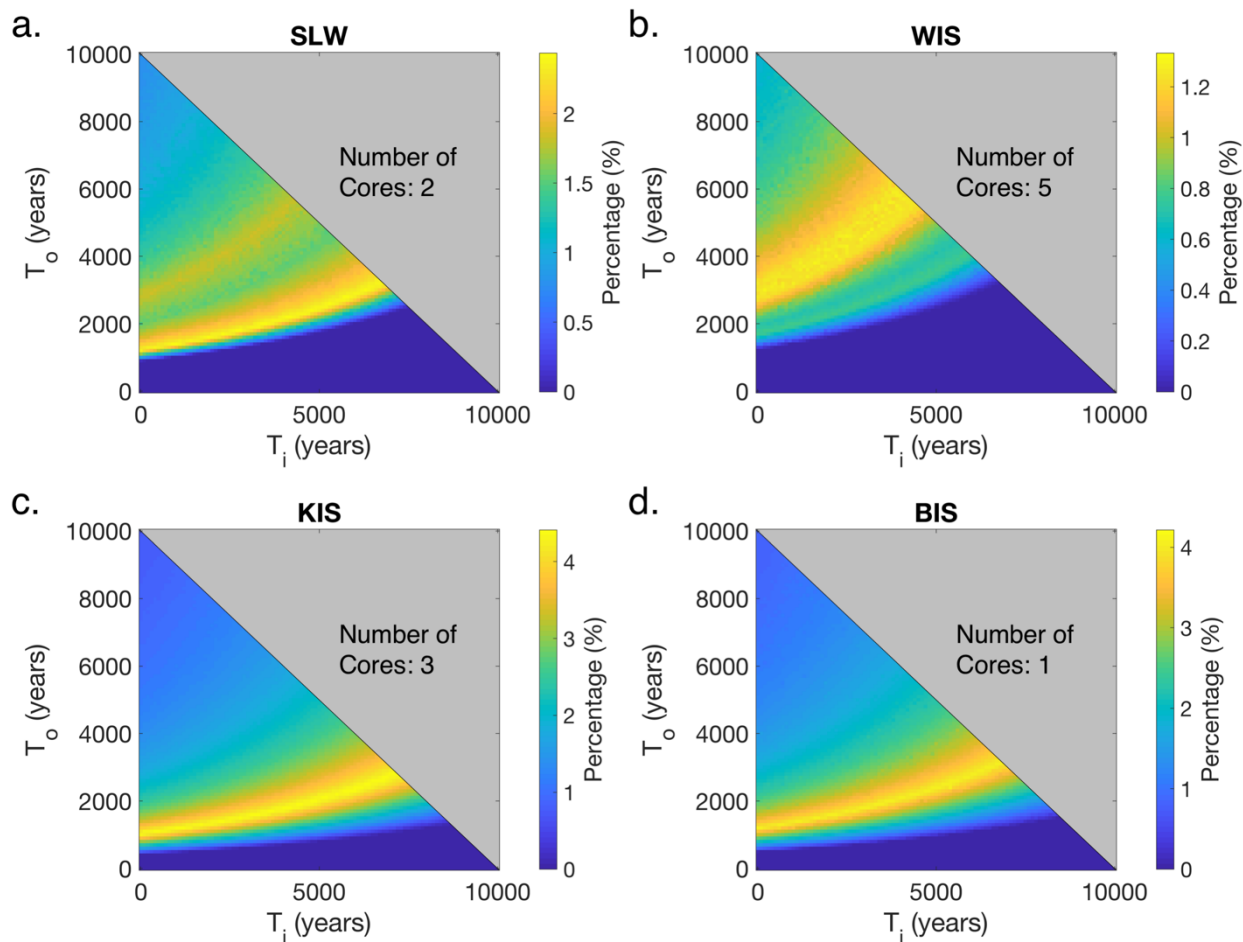
745

**Figure 4: Modelled basal temperature gradients given by the color scale in the background, compared to observed basal temperature gradients for KIS, BIS, and UC (Engelhardt, 2004). The observed basal temperature gradients are given as contour lines color-coded to their respective locations.**

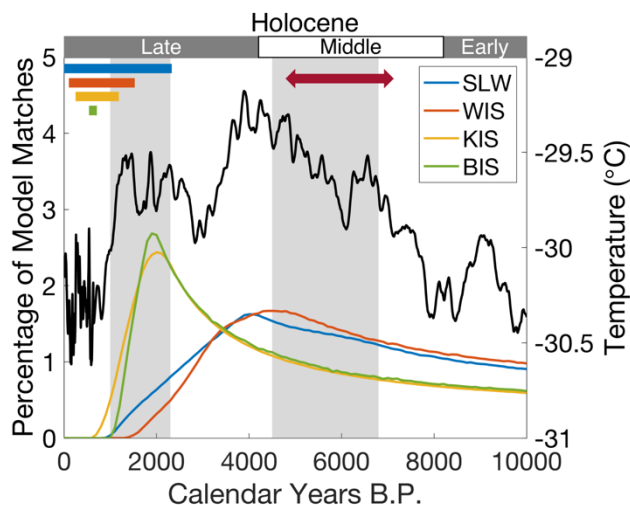


750

**Figure 5: Results from ionic diffusion modelling.  $T_o$  represents the length of time over which the topmost sediment was exposed to ocean water after initial grounding line retreat and before grounding line re-advance.  $T_i$  represents the length of time over which the topmost sediment was exposed to subglacial conditions between the grounding line re-advance over SLW and now.**



755 **Figure 6: Results of radiocarbon modelling for all eleven subglacial cores. The axes correspond to the length of time the grounding line position had either retreated behind the sites ( $T_o$ ) or advanced over them ( $T_i$ ). The percentage corresponds to the number of model runs which produced the simulated values of  $F_m$  and TOC, and which fit measured values for each core. The model runs for each core are stacked on top of each other, corresponding to their field site. (a) SLW (b) WIS (c) KIS (d) BIS.**



760 **Figure 7: The estimated timing of grounding line retreat and re-advance compared to selected climate data for the study region.**  
The colored lines represent the timing of grounding line retreat ( $T_o + T_i$ ) for each subglacial field site based on stacked results for  
each of the four subglacial locations. The solid bars in the upper left corner indicate the estimated time ranges over which the  
grounding line re-advanced over our field sites ( $T_i$ ). The black line represents the Holocene history of surface temperature at  
765 WAIS Divide (Cuffey et al., 2016; Cuffey, 2017). The gray vertical shaded regions indicate the warm periods of less extensive sea  
ice in the Western Ross Sea proposed by Hall et al. (2006), and the maroon arrow indicates the estimated range of grounding line  
retreat over WGZ based on the ramped-pyrolysis method (Venturelli et al., 2020).

770

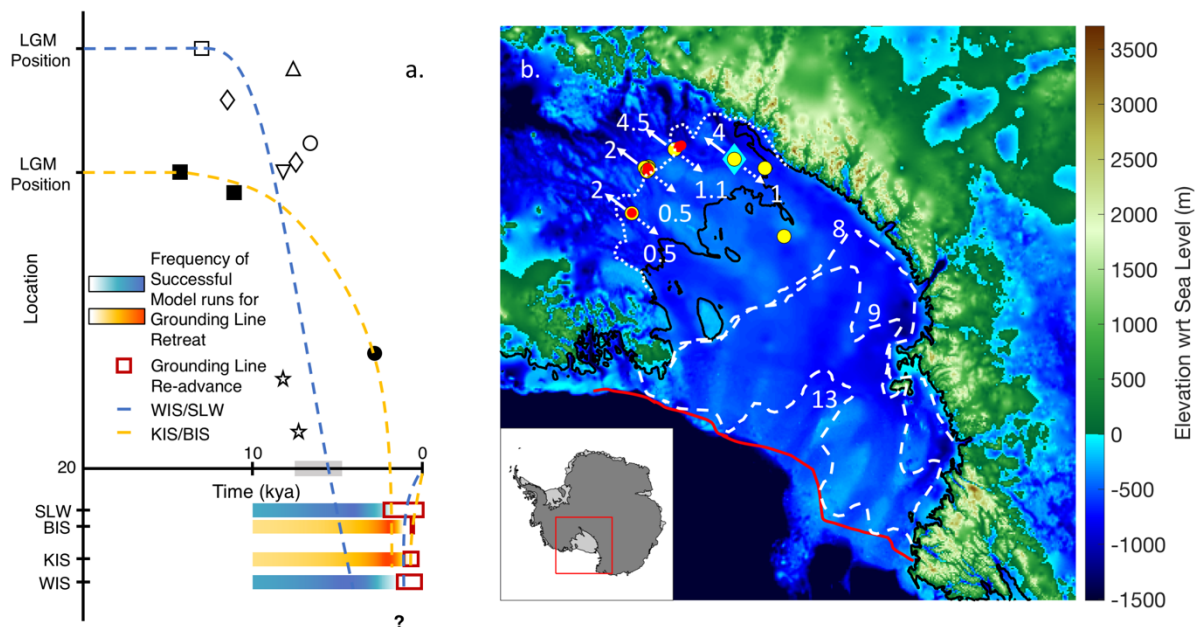


**Figure 8: The evolution of grounding line positions in the Ross Embayment for the past 20,000 years. (a) Schematic for grounding line position along the flow lines of the Whillans Ice Stream (blue dashed line) as well as the Bindschadler Ice Stream and Kamb Ice Stream (yellow dashed line). Symbols represent age constraints on grounding line position from the following studies: Baroni and Hall (2004) (right side up empty triangle), Bart et al. (2018) (solid square), Conway et al. (1999) (solid circle), Cunningham et al. (1999) (empty square), Jones et al. (2015) (empty circle), Licht et al. (1996) (empty diamond), McKay et al. (2016) (upside down empty triangle), Spector et al. (2017) (empty star). Open symbols represent ages along/near the flowline of the Whillans Ice Stream, and solid symbols represent ages along the flowline of the Bindschadler Ice Stream. Gray bar along the grounding line represents grounding line retreat at WGZ calculated in Venturelli et al. (2020). (b) Map-view of Holocene grounding line positions in the Ross Embayment. Background image is bed elevation (Fretwell et al., 2013). Yellow dots denote the location of sediment cores taken for radiocarbon and TOC analysis. Red dots denote the location of deep temperature profiles examined in this study. Cyan diamond indicates the location where sediment porewater was collected and analyzed. Red line indicates LGM grounding line position (Bentley et al., 2014). Dashed white lines indicate grounding line retreat from Lee et al. (2017). The corresponding numbers indicate timing in kya (thousands of years). Dotted white line shows most retreated grounding line position modelled in Kingslake et al. (2018). Solid white arrows indicate timing of grounding line retreat in kya, and dotted white arrows indicate timing of grounding line re-advance over those sites.**

775

780

785

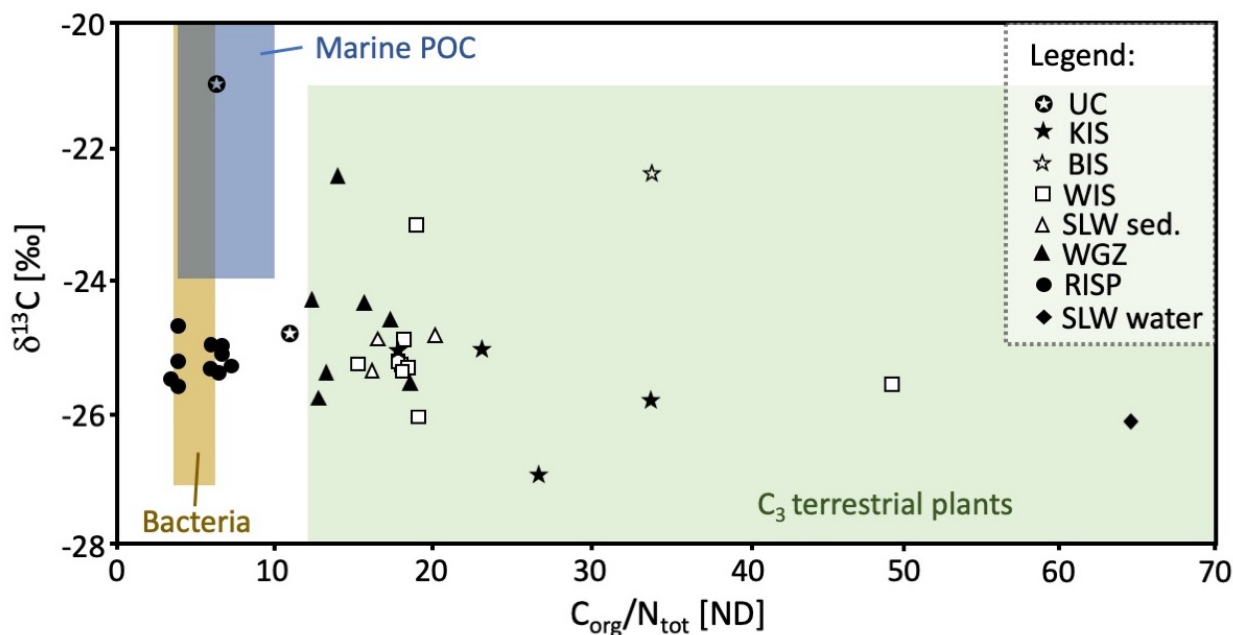


Figure 9:  $\delta^{13}\text{C}$  plotted against  $C_{\text{org}}:N_{\text{org}}$  (atom:atom). Shaded areas taken from Lamb et al. (2006). Although the RISP and WGZ samples are from a sub-ice shelf cavity, RISP is located mid-ice shelf whereas WGZ is located within the grounding zone. The UC samples are sediments melted out from basal ice, as opposed to collected below ice or an ocean cavity.

790

Table 1: Diffusion coefficients and concentrations for chemical parameters examined in the porewater diffusion model. The seawater concentrations are the typical concentrations in standard 35 per-mil seawater, and the meltwater concentrations are from measurements taken in Subglacial Lake Whillans (Michaud et al., 2016a).

Chemical Parameter	$D_{\text{sed}}$ ( $\text{m}^2/\text{yr}$ )	Seawater Concentration *(g/kg) or **(%o)	Meltwater Concentration *(g/kg) or **(%o)
$\text{Cl}^-$	0.0113	*19.353	*0.125
$\text{SO}_4^{2-}$	0.00557	*2.712	*0.053
$\text{Na}^+$	0.00699	*10.76	*0.121
$\text{Ca}^{2+}$	0.00416	*0.412	*0.017
$\delta^{18}\text{O} - (\text{H}_2\text{O})$	0.0162	**0	** -38
$\delta\text{D} - (\text{H}_2\text{O})$	0.0111	**0	** -300.9

795